ACS APPLIED MATERIALS & INTERFACES

Research Article

www.acsami.org

$NiS_{1.97}$: A New Efficient Water Oxidation Catalyst for Photoelectrochemical Hydrogen Generation

Reshma Bhosale,*[,†,‡] Sarika Kelkar,[†] Golu Parte,[§] Rohan Fernandes,[∥] Dushyant Kothari,[∥] and Satishchandra Ogale*[,†,‡,§]

[†]Physical and Materials Chemistry Division, National Chemical Laboratory, Pune 411008, India

[‡]Academy of Scientific and Innovative Research, Anusandhan Bhawan, 2 Rafi Marg, New Delhi 110001, India

[§]Indian Institute of Science Education and Research, Dr. Homi Bhabha Road, Pashan, Pune 411008, India

[∥]Department of Physics and National Centre for Nanosciences & Nanotechnology, University of Mumbai, Vidyanagri, Santacruz (E), Mumbai 400098, India

Supporting Information

ABSTRACT: $NiS_{1.97}$, a sulfur-deficient dichalcogenide, in nanoscale form, is shown to be a unique and efficient photoelectrochemical (PEC) catalyst for H_2 generation by water splitting. Phase pure $NiS_{1.97}$ nanomaterial is obtained by converting nickel oxide into sulfide by controlled sulfurization method, which is otherwise difficult to establish. The defect states (sulfur vacancies) in this material increase the carrier density and in turn lead to favorable band line-up with respect to redox potential of water, rendering it to be an effective photoelectrochemical catalyst. The material exhibits a remarkable PEC performance of 1.25 mA/cm^2 vs NHE at 0.68 V in neutral pH, which is almost 1000 times superior as compared with that of the stoichiometric phase of NiS_2. The latter is well-known to be a cocatalyst but not as a primary PEC catalyst.

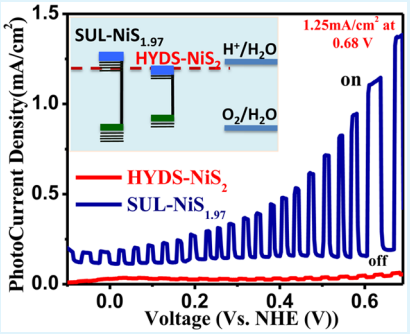

KEYWORDS: *$NiS_{1.97}$, dichlacogenide, nonstoichiometric, hydrogen generation, photoelectrochemical catalyst, sulfurization, Faradaic efficiency*

1. INTRODUCTION

Hydrogen is recognized as a highly promising fuel for the future.[1] Existing methods of hydrogen production on the commercial scale are neither economical nor clean, thereby defeating the very purpose for which we seek hydrogen energy technology.[2−5] There is thus a real and express need for exploring clean and efficient methods of H_2 generation. Toward this end, solar-driven water splitting is a very attractive proposition. During the past decade, a large number of material systems, mostly belonging to metal nitride and oxide families, have been studied and have demonstrated to render fairly good efficiencies and stability.[1,6] However, in the interest of even higher and commercially viable efficiencies, the search needs to be expanded to other promising classes of materials.

Metal dichalcogenides with pyrite structure (MX_2, where M = Fe, Co, Ni, Mo, and X = S, Se) are interesting materials to examine in this context because they are earth abundant and relatively inexpensive and have long-term stability in both acidic and basic media.[7,8] They also have a unique combination of optical and electronic properties that are suitable for the stated application. Most of dichacogenides absorb the visible solar spectrum with high absorption coefficient, and their electronic structure (energy gaps and optical emissions) can be tuned continuously by changing their stoichiometry, dimensionality, and size (quantum size effects). Moreover, their short carrier diffusion times, photochemical stability and electrical conductivity make them potentially appropriate candidates for efficient H_2 generation.[9]

From the metal sulfide family, cobalt sulfide (CoS) has been demonstrated to be an effective electrochemical and photoelectrochemical (PEC) catalyst for H_2 generation.[10] However, from the metal disulfide (dichalcogenide) family, materials such as CoS_2,[11] FeS_2,[12] MoS_2,[13] and NiS_2[14] have only been studied as electrocatalysts and not as a single light absorber PEC catalyst for water splitting. NiS_2 has proved to be a particularly effective electrocatalyst. It is a Mott-insulator with a band gap 0.3−0.8 eV and its surface is intrinsically metallic.[15] Pang et al.[14] have reported microwave assisted synthesis of NiS_2 nanospheres exhibiting enhanced photocatalytic performance for H_2 generation by employing erythrosin yellow system as the main photon absorber and triethanolamine as a sacrificial agent. Similarly, Yin et al.[16] have reported noble metal free NiS_2 nanoparticles as a cocatalyst for the g-C_3N_4 system wherein the corresponding loading was shown to improve the photocatalytic H_2 generation rate by inhibiting recombination of the photogenerated charge carriers. In none of these works NiS_2

Received: June 9, 2015
Accepted: August 28, 2015
Published: August 28, 2015

DOI: 10.1021/acsami.5b05077
ACS Appl. Mater. Interfaces 2015, 7, 20053−20060

has been examined or reported as a photoelectrode for PEC water splitting possibly because of the incompatibility of its band structure, vis a vis the water redox potentials.

We set out to synthesize this material in the form of a nanosystem so as to examine whether any property features could be tuned to render it effective in the context of the said objective of hydrogen evolution. When we synthesized NiS_2 nanoparticles by the hydrothermal method, metallic nickel Ni (0) contribution was revealed to be present in the surface layer by X-ray photoelectron spectroscopy (XPS). This material did not show any notable photoelectrochemical (PEC) water splitting. To get rid of the Ni (0), we sulfurized the sample and obtained NiS_2 phase. This sulfurized catalyst showed a slight gain in water splitting current density (about 7 $\mu A/cm^2$) but still not so significant. Interestingly, when we adopted another route to make NiS_2 film by first making NiO film by doctor blading followed by sulfurization, we obtained single phase $NiS_{1.97}$ which showed a dramatic increase in the current density of water splitting (over 1.25 mA/cm^2 vs NHE at 0.68 V).

In this study, we demonstrate for the first time a new facet of the nickel disulfide system, namely its efficacy as a photoelectrochemical catalyst, but only for its sulfur deficient phase $NiS_{1.97}$. We show that when synthesized under halogen vapor transport method, the sulfur deficient $NiS_{1.97}$ phase can be stabilized which has a favorable flat band potential and band line-up for water splitting as compared to NiS_2. It gives not only highly impressive PEC performance but also very good stability. Furthermore, this work highlights the role of surface defect states (nonstoichiometry) in rendering an efficient water splitting performance due to pinning of Fermi level, improved charge transport, and increased visible light absorption.

2. EXPERIMENTAL SECTION

2.1. Synthesis of HYD-NiS_2. NiS_2 was synthesized by modified hydrothermal process following previous reports[16] wherein it was used in PEC experiments but only as cocatalyst. Typically 0.1 g Nickel acetate tetrahydrate (Spectrochem, > 99%) was dissolved in 70 mL of deionized (DI) water followed by the addition of 8 g of thiourea (Sigma-Aldrich, > 99%) in 100 mL Teflon lined autoclave. Inside it, washed fluorine-doped tin oxide (FTO) was inserted vertically with the conducting side facing the wall of the autoclave at a slight slanting angle. The autoclave was kept at 140 °C for 8 h. After cooling to room temperature, the films were rinsed with water and dried in an oven.

2.2. Synthesis of HYDS-NiS_2. The surface layer of the above-mentioned hydrothermally synthesized HYD-NiS_2 sample was observed to have a strong contribution of Ni (0) state as confirmed from XPS (Supporting Information, Figure S3a) even though XRD showed pure NiS_2 phase. To remove or reduce the density of this Ni (0) surface state the HYD-NiS_2 sample was sulfurized to convert the material fully into sulfide form by heating in a furnace at 500 °C for 30 min at a ramp rate of 3 °C/min under the presence of sulfur source by using Ar as a carrier gas. The NiS_2 sample thus obtained after sulfurization is abbreviated as "HYDS-NiS_2".

2.3. Synthesis of SUL-$NiS_{1.97}$. Synthesis of SUL-$NiS_{1.97}$ involved three steps as follows:

2.3.1. Synthesis of Ni(OH)$_2$. In a typical experiment, 0.01 mol of $NiCl_2.6H_2O$ (Alfa Aesar, > 98%) was dissolved in 30 mL distilled water under magnetic stirring for 15 min to form a homogeneous solution at room temperature, and then 0.03 mol of NaOH (Merck, > 97%) dissolved in 15 mL of DI water was added dropwise to the above solution. The as-formed green colored Ni $(OH)_2$ precipitate was washed with 1 L of DI water. To this washed precipitate was added 0.01 mol NaOH dissolved in 30 mL of DI water.

This final solution was then transferred into a 50 mL Teflon-lined stainless steel autoclave, sealed, and maintained at 160 °C for 20 h, followed by natural cooling to room temperature. The product was collected, washed several times with distilled water and absolute ethanol, and dried at 60 °C in air.

2.3.2. Synthesis of NiO. The above obtained Ni$(OH)_2$ powder was calcined at 600 °C for 2 h at a ramp rate of 10 °C/min to obtain gray colored NiO powder, as shown in Figure 1. From this powder (0.2 g),

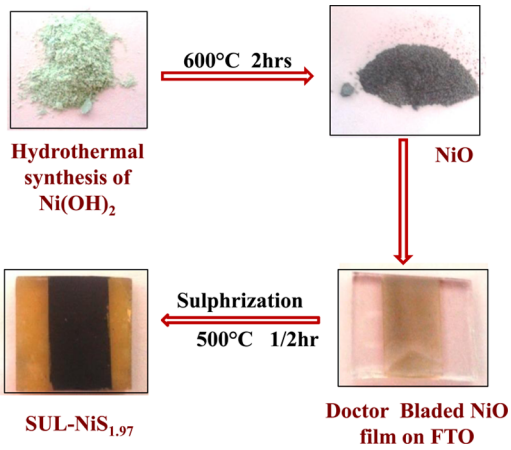

Figure 1. Synthesis protocol for SUL-$NiS_{1.97}$.

paste was prepared in a mortar by adding Triton X-100 (Thomas Baker, > 98%) and PEG (Sigma-Aldrich). This paste was coated on FTO by doctor blading method followed by heating at 450 °C for 1 h to obtain a film of thickness around 1−1.5 μm.

2.3.3. Sulfurization of NiO. NiO was sulfurized by the same parameters described earlier, and the obtained sample was abbreviated as SUL-$NiS_{1.97}$. The doctor bladed NiO film was kept inside a split-tube furnace connected to a sulfur source for sulfurization at 500 °C for 30 min at a ramp rate of 3 °C/min. The sulfur source was in the form of thioacetamide (Sigma-Aldrich, > 99%) which was heated at 200 °C and the vapor was carried into the furnace by using Ar as the carrier gas. The films were then taken out of the furnace after they cooled to room temperature naturally.

2.4. Characterization. Phase of powders Ni $(OH)_2$ and NiO along with all sulfide electrodes (on FTO) was confirmed by X-ray diffraction (XRD, Philips X' Pert PRO). Light absorption properties of sulfide electrodes were measured by diffuse reflectance spectroscopy (DRS Varian, CARY100). Photoluminescence spectra were obtained on Fluoromax-4, Spectrofluorometer (HORIBA scientific). Surface analysis was done by X-ray photoelectron spectroscopy (XPS) Phi 5000 Versa Probe 2 equipped with a monochromatic Al Kα (1486.6 eV) X-ray source and a hemispherical analyzer. Morphology of the samples was studied using field emission scanning electron microscope (FESEM, FEI Quanta 200 3D). N_2 gas adsorption−desorption measurements were performed using Quadrasorb automatic volumetric instrument at 77 K. The thickness of electrodes was measured by surface profiler from Dektak 150, Veeco. Mott−Schottky plots were recorded at a scan rate of 10 mV/s in Na_2SO_4 neutral solution in darkness at a frequency of 10 kHz.

The photoelectrochemical (PEC) measurements of sulfide electrodes were carried out in a three-electrode system using AUTOLAB PGSTAT 30. The photoanode material coated on FTO with 0.25 cm^2 area served as the working electrode, platinum foil as the counter electrode, and Ag/AgCl as the reference electrode in a 0.1 M Na_2SO_4 electrolyte (pH 7.4) under simulated sunlight illumination at100 mW/cm^2 from a 400 W xenon lamp. The measured potentials vs Ag/AgCl were converted to the standard hydrogen electrode (NHE) scale according to the Nernst equation:

$$E_{NHE} = E_{Ag/AgCl} + 0.1976V \quad (1)$$

where, E_{NHE} is the converted potential vs NHE, $E_{Ag/AgCl}$ = 0.1976 V at 25 °C, and $E_{Ag/AgCl}$ is the experimentally measured potential against the Ag/AgCl reference. To confirm that the photocurrents observed in

DOI: 10.1021/acsami.5b05077
ACS Appl. Mater. Interfaces 2015, 7, 20053−20060

the PEC cell are really due to PEC water splitting, we constructed a sealed and inert PEC system.

Chronoamperometry measurements (stability profile) were performed using a two-electrode method under the bias of 1.1 V up to 60 min. The amounts of O_2 and H_2 generated from the two compartments of the PEC systems were detected and quantified by headspace gas analysis with an Agilent 7890A Series Gas Chromatograph (GC) equipped with a 5°A molecular sieve column. Thermal conductivity detector (TCD) equipped GC was used. The two-electrode PEC system was kept in darkness initially for 30 min (control experiment), and then the photoanode was exposed to light from a solar simulator (100 mW/cm^2). The O_2 and H_2 were collected from anodic and cathodic compartments of the PEC cell, respectively, through a tightly sealed septum. Readings were recorded through GC at a 10 min interval.

3. RESULTS AND DISCUSSION

First, the nature of the Ni-sulfide phase obtained by the hydrothermal synthesis (named HYD-NiS_2) was ascertained by XRD (Supporting Information, Figure S1a), where no Ni (0) contribution is seen. However, as seen from the X-ray photoelectron spectroscopy (XPS) data for the same sample (Supporting Information, Figure S3a) a strong contribution of Ni (0) is noted, which required ex situ sulfurization. When HYD-NiS_2 sample was ex situ sulfurized to convert the Ni (0) surface to sulfide, the XRD of this sample (abbreviated as HYDS-NiS_2) shown in Figure 2a is found to be almost similar

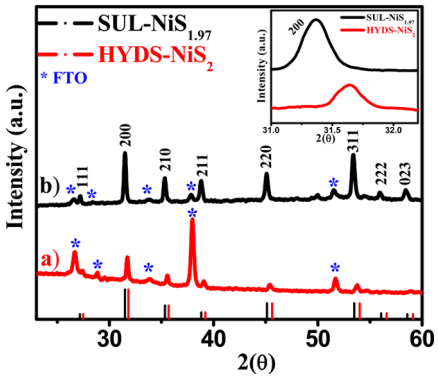

Figure 2. XRD pattern of (a) HYDS-NiS_2 and (b) SUL-$NiS_{1.97}$; peaks marked by an asterisk (*) correspond to the FTO substrate.

to the HYD-NiS_2. The 2(θ) values are 27.5, 31.7, 35.5, 39.0, 45.5, and 53.8°, which match with JC-PDF 80-0375, indicating pure NiS_2 phase. However, as discussed later with the help of XPS result, the ex situ sulfurization reduced the Ni(0) contribution dramatically, as desired. The peaks marked by an asterisk (*) correspond to the FTO substrate. Due to the thin film character of this HYDS-NiS_2 sample, the FTO peaks are more intense than the NiS_2 peaks.

The third sample for the experiment, namely $NiS_{1.97}$ in nanoparticulate form, was obtained by the procedure explained in the Experimental Section starting from $Ni(OH)_2$ which was converted to NiO followed by sulfurization of the NiO film. The XRD pattern of $Ni(OH)_2$ and NiO powders are also given in the Supporting Information (Figure S1b and c).

Thermal sulfurization of the doctor-bladed NiO film led to an XRD pattern as shown in Figure 2b. The peaks appearing at 2θ values of 31.4, 35.3, 38.6, 45.0, and 53.4° can be uniquely identified with the sulfur deficient $NiS_{1.97}$ phase (JC-PDF 330754 data). It may be noted that the peaks corresponding to the SUL-$NiS_{1.97}$ phase are clearly down shifted (as shown in the inset) with respect to the peak positions corresponding to the stoichiometric NiS_2 phase, confirming expanded lattice (larger lattice parameters) due to sulfur deficiency.

The band gaps of $NiS_{1.97}$ and HYDS-NiS_2 were estimated using Tauc plots given in Figure 3 based on the diffuse

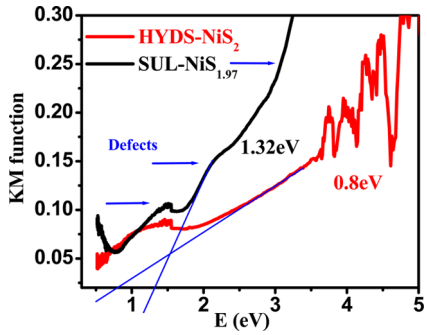

Figure 3. Tauc plots for SUL-$NiS_{1.97}$ and HYDS-NiS_2.

reflectance spectroscopy (DRS) data (Supporting Information, Figure S2). From the Tauc's plots the band gap of HYDS-NiS_2 is found to be 0.8 eV, as expected, and that of SUL-$NiS_{1.97}$ is found to be higher, namely 1.32 eV. The higher band gap of SUL-$NiS_{1.97}$ can be ascribed to changes in the electronic structure of NiS_2 due to a large concentration of sulfur vacancies. Notably, the corresponding changes in the electronic state density are seen to occur in the energy range of 1.5−2 eV due to defects resulting from nonstoitiometric nature of $NiS_{1.97}$.[17]

The presence of defects (S-vacancy states) in the SUL-$NiS_{1.97}$ sample can be further elucidated by room temperature photoluminescence (PL) spectroscopy. When the sample is excited at 380 nm, an emission peak is obtained at 418 nm, as shown in Figure 4. This peak can be strictly attributed to the

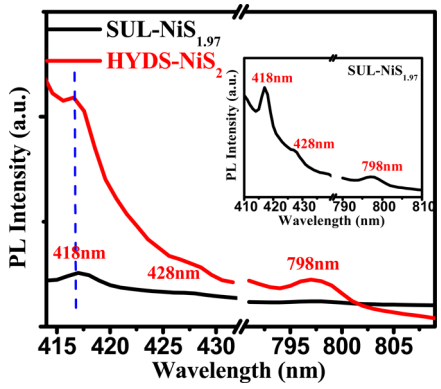

Figure 4. Photoluminescence (PL) spectra for SUL-$NiS_{1.97}$ and HYDS-NiS_2.

sulfur vacancy or interstitial sulfur lattice defects.[18] Another broad peak is located at 428 nm (Figure 4 inset), and the presence of such separated multiple peaks are an indication of structural defects within the sample due to electronic transitions, as discussed in the literature.[17,19] These peak positions are seen in both samples, indicating the same surface features, but the intensity of PL peak in case of SUL-$NiS_{1.97}$ is greatly reduced as compared to HYDS-NiS_2 indicating greater concentration of defects.

DOI: 10.1021/acsami.5b05077
ACS Appl. Mater. Interfaces 2015, 7, 20053−20060

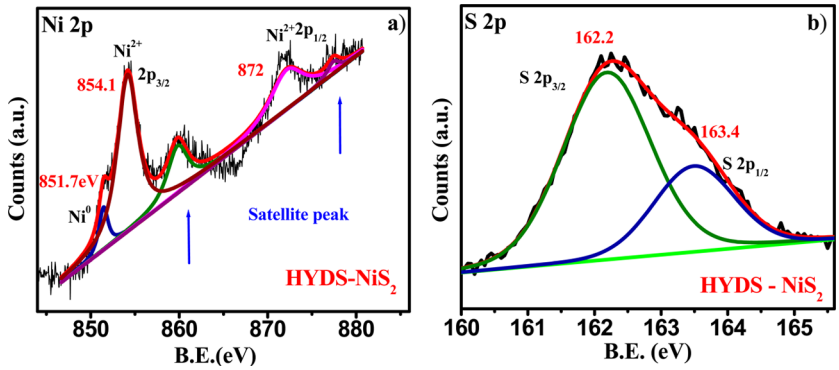

Figure 5. XPS spectra for HYDS-NiS_2: (a) Ni 2p contribution, (b) S 2p contribution.

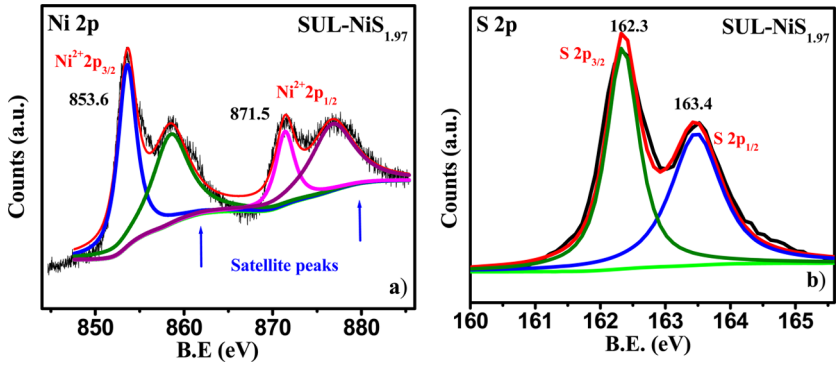

Figure 6. XPS spectra of SUL-$NiS_{1.97}$: (a) Ni 2p contribution, (b) S 2p contribution.

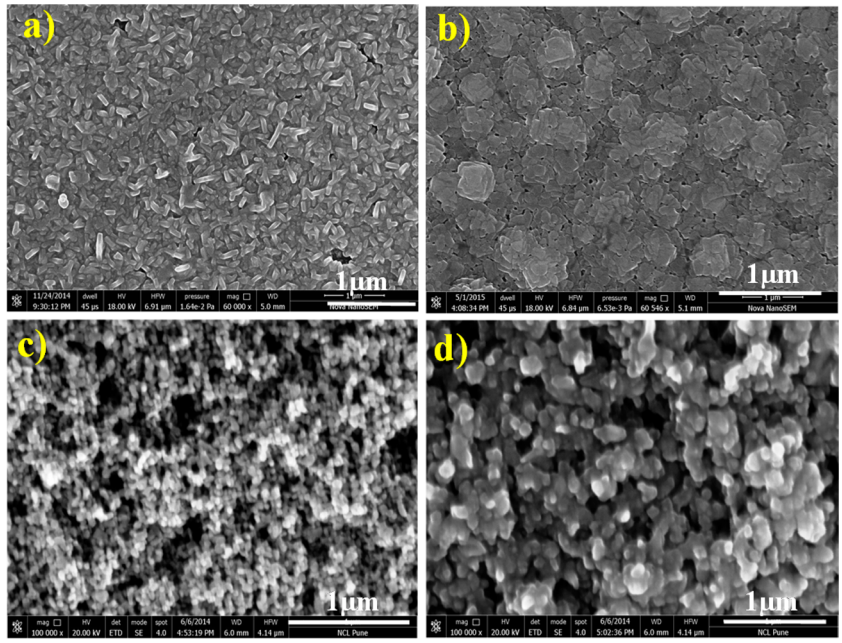

Figure 7. FESEM images of (a) HYD- NiS_2, (b) HYDS-NiS_2, (c) NiO, and (d) SUL-$NiS_{1.97}$.

The reduced PL intensity in diachalcogenide family (WS_2 and $MoSe_2$) has been investigated by Piemyoo et al.[20] and Wang et al.,[21] respectively.These authors have shown that defects, particularly anion (S) deficiency in the system, is the primary reason for quenching in intrinsic PL because such defects act as nonradiative recombination sites. Tongay et al.[22] reported that the sulfur vacancy creates energy levels near the band edges in the dichacogenide family and such defect-induced levels arising from nonstichiometry in the crystal system can influence the location of the Fermi level and thereby the PEC performance.[23] Also, a broad peak of low intensity is seen at 798 nm which can be attributed to intraband transitions in the $NiS_{1.97}$ band structure.[19]

Although the XRD pattern confirms the presence of pyrite phase, evaluation of surface chemistry (valence states) and the composition are of utmost importance in the context of the

DOI: 10.1021/acsami.5b05077
ACS Appl. Mater. Interfaces 2015, 7, 20053−20060

present work as these specifically control the phenomenon of photocatalysis.

Figure 5a shows the Ni 2p XPS spectrum of HYDS-NiS_2 sample. The peaks at 854.1 and 872 eV represent the Ni^{2+} state ($2p_{3/2}$ and $2p_{1/2}$ main lines). The two shake up-satellite peaks are found at 860 and 879 eV, respectively, for each of the emission lines of Ni 2p.[24] One more small peak at 851.7 eV is present indicating small amount of Ni (0) state at surface.[25] As stated earlier, this peak is present as a major contribution in the XPS spectrum of the HYD-NiS_2 sample (Supporting Information, Figure S3). After sulfurization, this contribution is reduced significantly, as desired. The sulfur contribution to the XPS spectrum of the HYDS-NiS_2 sample is given in Figure 5b. The two broad peaks at 162.2 and 163.4 eV are attributed to the S $2p_{3/2}$ and S $2p_{1/2}$ contributions. These indicate the presence of S_2^{2-} type of species (dimer of sulfur) which is bonded to Ni^{2+}.[24−26]

Figure 6a shows the XPS spectrum for the $NiS_{1.97}$ nanoparticulate sample (SUL-$NiS_{1.97}$). The peaks at 853.6 and 871.5 eV once again correspond to Ni $2p_{3/2}$ and Ni $2p_{1/2}$ contributions, respectively, representing the Ni^{2+} state. Interestingly, no discernible Ni (0) contribution is seen in this sample even though there is sulfur deficiency.

Figure 6b shows the sulfur contribution to the XPS spectrum of the SUL-$NiS_{1.97}$ sample. In this case the two peaks are again observed at 162 and 163 eV, corresponding to S $2p_{3/2}$ and S $2p_{1/2}$ binding energies, but they are significantly sharper than their counterparts in the case of HYDS-NiS_2 sample (Figure 5b). This indicates that the surface quality of the $NiS_{1.97}$ sample in terms of the uniformity of stoichiometry and possibly the crystalline quality is superior to that of HYDS-NiS_2. The Ni:S atomic ratios calculated from the corrected peaks obtained from the respective XPS spectra also show a significant difference. Here, it may be noted that the depth scale of the XPS probe is about 5−10 nm, and therefore, the ratios in the case of nanomaterials are not too precise but can only give a semiqualitative picture. The HYDS-NiS_2 sample showed the Ni:S ratio to be 1:2.4 indicating full sulfurization, whereas the SUL-$NiS_{1.97}$ sample showed the Ni:S ratio to be 1:1.7 confirming significant deficiency of sulfur. Such deficiency leads to defect states that can cause the decrease of PL intensity, as indeed seen in our case (Figure 4). It is reported by Wang et al.[27] that such sulfur deficiency (SV_s) on the surface acts as electron donor and induces localized (defect) states in the band gap. This in turn increases the carrier/donor density of the system which ultimately has a strong effect on pinning of the Fermi level.

In Figure 7, the FESEM images of the photoanodes HYD-NiS_2, HYDS-NiS_2, NiO and SUL- $NiS_{1.97}$ are given. In the image of Figure 7a, corresponding to the hydrothermally synthesized film, a granular morphology is seen which is much more compact. When this sample is thermally sulfurized the obtained HYDS-NiS_2 again shows a compact film of regularly fused nanoparticles as seen from FESEM image of Figure 7b. The FESEM image of NiO film is included specifically to show the morphology evolution upon sulfurization. In Figure 7c agglomerates of NiO nanoparticles of the size 50−60 nm are seen. This film when sulfurized gives SUL-$NiS_{1.97}$ with increased grain size of ∼120 nm, as shown in Figure 7d.The corresponding film is seen to be much more porous, which is beneficial for electrolyte contact, as the foremost rule of thumb for catalysis is the contact of the photocatalyst with the electrolyte/water. The BET surface area of SUL-$NiS_{1.97}$ is found to be 82 m^2/g, while that of HYDS-NiS_2 is found to be 69 m^2/g.

The data of the PEC measurements ($J-V$ scans) for the main two samples of interest (SUL-$NiS_{1.97}$ and HYDS-NiS_2) are presented in Figure 8. It is useful to mention here that the

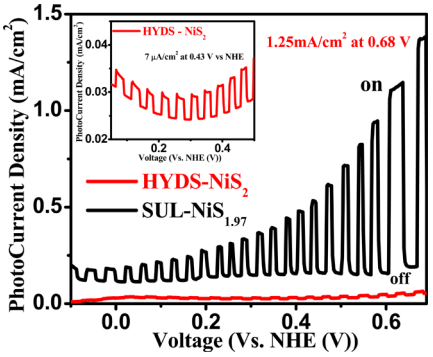

Figure 8. Photoelectrochemical measurement ($J-V$ scans) data for SUL-$NiS_{1.97}$ and HYDS-NiS_2 (Inset is enlarged view).

sample HYD-NiS_2 shows almost no photo effect (Supporting Information, Figure S4), but the sulfurized HYDS-NiS_2 sample showed a weak performance reflected by a current density of about 7 $\mu A/cm^2$ (see inset to Figure 8). Most interestingly, however, the sulfide photoanode SUL-$NiS_{1.97}$ obtained by sulfurization of doctor bladed NiO film shows a remarkable photocurrent density of about 1.25 mA/cm^2 at 0.68 V vs NHE. It is important to emphasize that the SUL-$NiS_{1.97}$ sample shows the stated impressive performance as a main PEC catalyst without any additional cocatalyst in neutral pH with a low applied bias of 0.68 V. It may further be noted that the observed orders of magnitude difference in performance between the HYDS-NiS_2 and SUL-$NiS_{1.97}$ samples cannot be accounted for by only about 19% higher surface area of the latter over the former. Thus, the differences in the electronic states of the two materials and the corresponding implications for band alignments hold the key.

To bring out and elucidate the possible reasons for such high PEC performance and its possible correlation to the defect induced electronic states, Mott−Schottky analysis was done. First, the plot given in Figure 9 shows a positive slope for both the sulfide electrodes indicating their n- type semiconductor character. Second, the Flat band (fb) potential estimated from the x intercept of the linear portion of the Mott−Schottky plots, indicates that the Fb-potential of $NiS_{1.97}$ is −0.33 V and

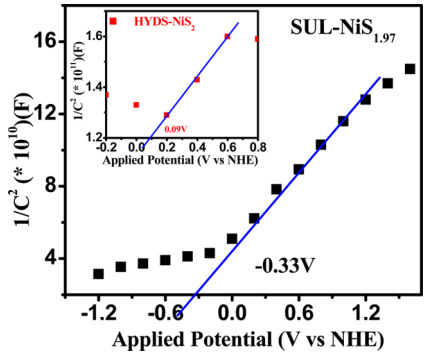

Figure 9. Mott−Schottky plots of SUL-$NiS_{1.97}$ and HYDS-NiS_2 (inset).

DOI: 10.1021/acsami.5b05077
ACS Appl. Mater. Interfaces 2015, 7, 20053−20060

that of HYDS-NiS_2 is 0.09 V. The Fb-potential of HYD-NiS_2 is 0.29 V (Supporting Information, Figure S5). From the flat band potential and the band gap calculated from the Tauc's plot approximate energy levels were determined which could reveal a clear picture as to why $NiS_{1.97}$ shows 2−3 orders of magnitude superior photocatalytical activity as a single absorbing anode material as compared to NiS_2. This is clearly because the conduction-band edge of SUL-$NiS_{1.97}$ is just above the hydrogen-evolution potential, and the edge of the valence band lies below the oxygen-evolution potential of water as shown schematically in Scheme 1. This makes the charge transfer reactions for water splitting feasible.

Scheme 1. Schematic Diagram of Energy Levels of Photoanodes

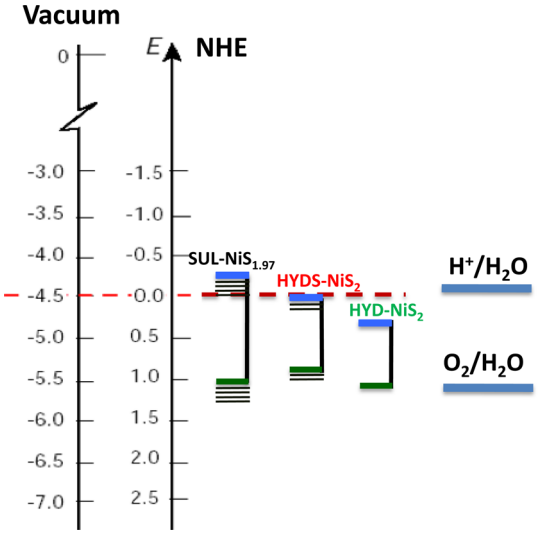

Also, the introduced defect levels below the band edges must be electronically active to perform charge transfer and redox reactions in water. On the other hand, the hydrothermally synthesized and sulfurized HYDS-NiS_2 sample and the only hydrothermally synthesized sample do not have such desirable band alignment to facilitate the water splitting process. The HYDS-NiS_2 sample has some degree of advantage in this respect as compared to the HYD-NiS_2 sample and as such shows a degree of water splitting which is totally absent for the HYD-NiS_2 case. Notably, the hydrothermally synthesized but unsulfurized sample HYD-NiS_2 has much more positive conduction band edge which has established it as an efficient cocatalyst instead of PEC catalyst.

From the Mott−Schottky plots, we calculated the slopes for two samples, which are inversely proportional to the carrier density values. The charge carrier density can be calculated from eq 1 as follows.[28]

$$N_d = (2/e_0\varepsilon\varepsilon_0)[d(1/C_2)/dV]^{-1} \quad (2)$$

where N_d is carrier density, C is capacitance (F/cm^2), e_0 was the electron charge, ε is the dielectric constant, and ε_0 is permittivity of vacuum. The dielectric constant of NiS_2 is 6.52.[29] The calculated carrier density value for HYD-NiS_2 is 4.4 × 10^{17} cm^{-2}, HYDS-NiS_2 is 2.7 × 10^{18} cm^{-2} and SUL-$NiS_{1.97}$ is 3.6 × 10^{18} cm^{-2}. The SUL-$NiS_{1.97}$ sample clearly has a considerably higher carrier density than the other two NiS_2 samples. These data provide direct evidence that increased donor density in the SUL-$NiS_{1.97}$ sample is due to S-vacancy which is also consistent with the PL and XPS analyses. This increased donor density causes upward shift of Fermi level making the levels favorable with regard to the redox potential of water, as also seen in the case of TiO_2 system.[30] Moreover, this increased donor density also promotes band bending at the surface.[31] This band bending along with the induces defect levels facilitate better charge separation and transport across the electrode/electrolyte interface making $NiS_{1.97}$ nanosystem to be an efficient photoelectrochemical catalyst operating at lower bias voltage in neutral pH without need of any cocatalyst.

Figure 10 shows the chronoamperometry data (stability profile) for the SUL-$NiS_{1.97}$ sample which exhibits an almost

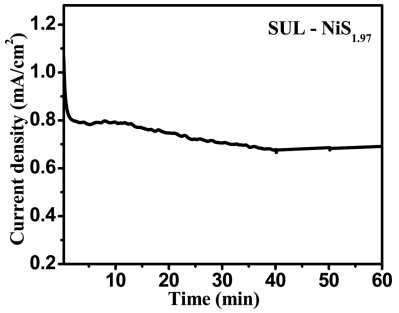

Figure 10. Chronoamperometry profile for SUL-$NiS_{1.97}$.

stable current density of 0.83 mA/cm^2 for 60 min when bias of 1.1 V is applied between the working and counter electrode. This stability profile (in terms of current density) was used for theoretical calculation of the expected gas evolution rates. Figure 11 compares the theoretically expected and experimental

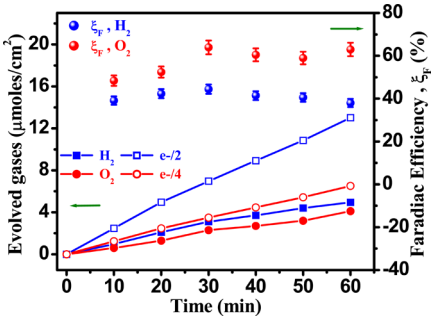

Figure 11. Theoretical and measured gas production rates of (□) H_2, (○) O_2 and (■) H_2, (●) O_2, respectively, along with (spheres) the Faradiac efficiency for SUL-$NiS_{1.97}$.

found (by GC analysis) quantities of hydrogen and oxygen evolved as a function of time. The ratio of the measured and calculated gas evolution rates gives the Faradiac efficiency at 1.1 V. The efficiency is close to about 65% for oxygen, but is relatively lower (about 40−45%) for hydrogen evolution. This suggests some losses by side or back reactions along with thermal losses. This efficiency could be improved by further optimization of the catalyst material, the applied bias and by passivating the catalyst surface to inhibit deleterious (side) reactions.

4. CONCLUSION

From the dichalcogenide family, the sulfur deficient $NiS_{1.97}$ phase is established for the first time as an efficient water oxidation catalyst for photoelectrochemical (PEC) catalyst for

DOI: 10.1021/acsami.5b05077
ACS Appl. Mater. Interfaces 2015, 7, 20053−20060

water splitting. This phase is realized following a specific synthetic protocol and thermal sulfurization method. The S-vacancy mediated single phase material renders electronic states which yield a positioning of the Fermi level and the conduction/valence bands vis a vis the water redox levels, which are favorable for water splitting. This leads to a remarkable order of magnitude superior water splitting performance of $NiS_{1.97}$ over NiS_2, the latter established only as a cocatalyst until now. This study brings out a defect engineering strategy for tuning the properties of (di)-chalcogenides photoanodes for enhancing the water splitting ability and, in a broader context, for enhancing their applicability to other optoelectronic property domains.

■ ASSOCIATED CONTENT

Supporting Information

The Supporting Information is available free of charge on the ACS Publications website at DOI: 10.1021/acsami.5b05077.

XRD of HYD-NiS_2, $Ni(OH)_2$ and NiO, DRS and XPS of HYD-NiS_2,PEC performance of HYD-NiS_2, Mott–Schottky of HYD-NiS_2 (PDF)

■ AUTHOR INFORMATION

Corresponding Authors

*E-mail: satishogale@gmail.com.
*E-mail: reshmabhosale10@gmail.com.

Author Contributions

The manuscript was written through contributions of all authors, though most of the experimental work was performed by R.B. All authors have given approval to the final version of the manuscript.

Notes

The authors declare no competing financial interest.

■ ACKNOWLEDGMENTS

R.B. would like to thank CSIR for fellowship support. Authors would also like to thank CSIR-TAPSUN program and Dr. Deodatta Phase and Dr. Ram Choudhary for experimental help.

■ REFERENCES

(1) Bak, T.; Nowotny, J.; Rekas, M.; Sorrell, C. C. Photo-electrochemical Hydrogen Generation from Water using Solar energy. Materials -Related Aspects. *Int. J. Hydrogen Energy* **2002**, *27*, 991–1022.

(2) Navarro, R. M.; Pena, M. A.; Fierro, J. L. G. Hydrogen Production Reactions from Carbon Feedstocks: Fossil Fuels and Biomass. *Chem. Rev.* **2007**, *107*, 3952–3991.

(3) Palo, D. R. Methanol Steam Reforming for Hydrogen Production. *Chem. Rev.* **2007**, *107*, 3992–4021.

(4) Rostrup-Nielsen, J. R.; Sehested, J. S.; Norskov, J. K. Hydrogen and Synthesis Gas by Steam- and C0$_2$ Reforming. *Adv. Catal.* **2002**, *47*, 65–139.

(5) Bockris, J. O. M. The Origin of Ideas on a Hydrogen Economy and its Solution to the Decay of the Environment. *Int. J. Hydrogen Energy* **2002**, *27*, 731–740.

(6) Navarro Yerga, R.M. N.; Álvarez Galvan, M. C.; del Valle, F.; Villoria de la Mano, J. A.; Fierro, J. L. G. Water Splitting on Semiconductor Catalysts under Visible- Light Irradiation. *ChemSusChem* **2009**, *2*, 471–485.

(7) Kong, D.; Cha, J. J.; Wang, H.; Lee, H. R.; Cui, Y. First-row Transition metal Dichalcogenide Catalysts for Hydrogen Evolution Reaction. *Energy Environ. Sci.* **2013**, *6*, 3553–3558.

(8) Faber, M. S.; Dziedzic, R.; Lukowski, M. A.; Kaiser, N. S.; Ding, Q.; Jin, S. High-Performance Electrocatalysis Using Metallic Cobalt Pyrite (CoS_2) Micro- and Nanostructures. *J. Am. Chem. Soc.* **2014**, *136*, 10053–10061.

(9) Singh, N.; Jabbour, G.; Schwingenschlogl, U. Optical and Photocatalytic Properties of Two-Dimensional MoS_2. *Eur. Phys. J. B* **2012**, *85* (392), 1–4.

(10) Sun, Y.; Liu, C.; Grauer, D. C.; Yano, J.; Long, J. R.; Yang, P.; Chang, C. J. Electrodeposited Cobalt-Sulfide Catalyst for Electrochemical and Photoelectrochemical Hydrogen Generation from Water. *J. Am. Chem. Soc.* **2013**, *135*, 17699–17702.

(11) Faber, M. S.; Lukowski, M. A.; Ding, Q.; Kaiser, N. S.; Jin, S. Earth-Abundant Metal Pyrites (FeS_2, CoS_2, NiS_2, and Their Alloys) for Highly Efficient Hydrogen Evolution and Polysulfide Reduction Electrocatalysis. *J. Phys. Chem. C* **2014**, *118*, 21347–21356.

(12) Du, P.; Eisenberg, R. Catalysts made of Earth-abundant elements (Co, Ni, Fe) for Water splitting: Recent Progress and Future Challenges. *Energy Environ. Sci.* **2012**, *5*, 6012–6021.

(13) Chen, Z.; Forman, A. J.; Jaramillo, T. F. Bridging the Gap Between Bulk and Nanostructured Photoelectrodes: The Impact of Surface States on the Electrocatalytic and Photoelectrochemical Properties of MoS_2. *J. Phys. Chem. C* **2013**, *117*, 9713–9722.

(14) Pang, H.; Wei, C.; Li, X.; Li, G.; Ma, Y.; Li, S.; Chen, J.; Zhang, J. Microwave-assisted Synthesis of NiS_2 Nanostructures for Supercapacitors and Cocatalytic Enhancing Photocatalytic H_2 Production. *Sci. Rep.* **2014**, *4* (3577), 1–8.

(15) Rao, K. D. M.; Bhuvana, T.; Radha, B.; Kurra, N.; Vidhyadhiraja, N. S.; Kulkarni, G. U. Metallic Conduction in NiS_2 Nanocrystalline Structures. *J. Phys. Chem. C* **2011**, *115*, 10462–10467.

(16) Yin, L.; Yuan, Y. P.; Cao, S. W.; Zhang, Z.; Xue, C. Enhanced Visible-Light-Driven Photocatalytic Hydrogen Generation Over g-C_3N_4 Through Loading the Noble Metal-free NiS_2 Cocatalyst. *RSC Adv.* **2014**, *4*, 6127–6132.

(17) Linganiso, E. C.; Mhlanga, S. D.; Coville, N. J.; Mwakikunga, B. W. Size-dependent and Intra-Band Photoluminescence of NiS_2 Nano-Alloys Synthesized by Microwave Assisted Hydrothermal Technique. *J. Alloys Compd.* **2013**, *552*, 345–350.

(18) Li, Y.; Wang, H.; Zhang, H.; Liu, P.; Wang, Y.; Fang, W.; Yang, H.; Li, Y.; Zhao, H. A {0001} Faceted Single Crystal NiS Nanosheet Electrocatalyst for Dye-Sensitised Solar Cells: Sulfur-Vacancy Induced Electrocatalytic Activity. *Chem. Commun.* **2014**, *50*, 5569–5571.

(19) Akbarzadeh, R.; Dehghani, H.; Behnoudnia, F. Sodium Thiosulfate-Assisted Synthesis of NiS_2 Nanostructure by Using Nickel (II)-Salen Precursor: Optical and Magnetic Properties. *Dalton Trans.* **2014**, *43*, 16745–16753.

(20) Peimyoo, N.; Shang, J.; Cong, C.; Shen, X.; Wu, X.; Yeow, K. L.; Yu, T. Nonblinking, Intense Two-Dimensional Light Emitter: Monolayer WS_2 Triangles. *ACS Nano* **2013**, *7*, 10985–10994.

(21) Wang, X.; Gong, Y.; Shi, G.; Chow, W. L.; Keyshar, K.; Ye, G.; Vajtai, R.; Lou, J.; Liu, Z.; Ringe, E.; Tay, B. K.; Ajayan, P. M. Chemical Vapor Deposition Growth of Crystalline Monolayer $MoSe_2$. *ACS Nano* **2014**, *8*, 5125–5131.

(22) Tongay, S.; Suh, J.; Ataca, C.; Fan, W.; Luce, A.; Kang, J. S.; Liu, J.; Ko, C.; Raghunathanan, R.; Zhou, J.; Ogletree, F.; Li, J.; Grossman, J. C.; Wu, J. Defects Activated Photoluminescence in Two-Dimensional Semiconductors: Interplay between bound, charged, and Free Excitons. *Sci. Rep.* **2013**, *3* (2657), 1–4.

(23) Goswami, Y. *Advances in Solar Energy*, Vol *17*, American Solar Energy Society, Inc., Boulder, CO, 2007; p 179.

(24) Yang, S. L.; Yao, H. B.; Gao, M. R.; Yu, S. H. Monodisperse Cubic Pyrite NiS_2 Dodecahedrons and Microspheres Synthesized by a Solvothermal Process in a Mixed Solvent: Thermal Stability and Magnetic Properties. *CrystEngComm* **2009**, *11*, 1383–1390.

(25) Galtayries, A.; Bonnelle, J.-P. XPS and ISS Studies on the Interaction of H_2S with Polycrystalline Cu, Cu_2O and CuO Surfaces. *Surf. Interface Anal.* **1995**, *23*, 171–179.

(26) Smart, R. S. C.; Skinner, W. M.; Gerson, A. R. XPS of Sulphide Mineral Surfaces: Metal-Deficient, Polysulphides, Defects and Elemental Sulphur. *Surf. Interface Anal.* **1999**, *28*, 101–105.

(27) Qiu, H.; Xu, T.; Wang, Z.; Ren, W.; Nan, H.; Ni, Z.; Chen, Q.; Yuan, S.; Miao, F.; Song, F.; Long, G.; Shi, Y.; Sun, L.; Wang, J.; Wang,

DOI: 10.1021/acsami.5b05077
ACS Appl. Mater. Interfaces 2015, 7, 20053–20060

X. Hopping Transport Through Defect-Induced Localized States in Molybdenum Disulphide. *Nat. Commun.* **2013**, *4* (2642), 2642.
(28) Ling, Y.; Wang, G.; Wheeler, D. A.; Zhang, J. Z.; Li, Y. Sn-Doped Hematite Nanostructures for Photoelectrochemical Water Splitting. *Nano Lett.* **2011**, *11*, 2119.
(29) Anand, J. S.; Rajan, R. K. M.; Mohd Zaidan, A. A. Electrosynthesized NiS_2 Thin Films and their Optical and Semiconductor studies. *Rep. Electrochem.* **2013**, *3*, 25−29.
(30) Hu, Y. H. A Highly Efficient Photocatalyst—Hydrogenated Black TiO_2 for the Photocatalytic Splitting of Water. *Angew. Chem., Int. Ed.* **2012**, *51*, 12410−12412.
(31) Cui, H.; Zhao, W.; Yang, C.; Yin, H.; Lin, T.; Shan, Y.; Xie, Y.; Gu, H.; Huang, F. Black TiO_2 Nanotube Arrays for High-efficiency Photoelectrochemical Water-Splitting. *J. Mater. Chem. A* **2014**, *2*, 8612−8616.

DOI: 10.1021/acsami.5b05077
ACS Appl. Mater. Interfaces 2015, 7, 20053−20060